Progress in Additive Manufacturing (2022) 7:765–783
https://doi.org/10.1007/s40964-022-00264-z

FULL RESEARCH ARTICLE

Bio-composites for fused filament fabrication: effects of maleic anhydride grafting on poly(lactic acid) and microcellulose

Daniele Rigotti[1] · **Luca Fambri**[1] · **Alessandro Pegoretti**[1]

Received: 8 September 2021 / Accepted: 10 January 2022 / Published online: 24 January 2022

Abstract

Composite filaments consisting of poly(lactic acid) (PLA) and micro crystalline cellulose (MCC) were successfully used for additive manufacturing (AM) by fused filament fabrication (FFF). PLA and MCC bio-composites were obtained by direct mixing in a melt compounder; maleic anhydride (MAH) was also grafted onto PLA in reactive mixing stage to evaluate its effect on the final properties of the printed material. Filaments with various concentrations of MCC (up to a maximum content of 10 wt%) were produced with a single screw extruder and used to feed a commercial desktop FFF printer. Upon grafting of PLA with MAH, a more coherent interfacial morphology between PLA and MCC was detected by electron microscopy analysis. The thermal degradation of the PLA was unaffected by the presence of MCC and MAH. According to differential scanning calorimetry and dynamic mechanical analysis results, micro-cellulose acted as nucleating agent for PLA. In fact, the crystallization peak shifted towards lowers temperature and a synergistic effect when MCC was added to PLA grafted with MAH was observed possibly due to the increase of the chain mobility. Micro-cellulose led to an increase in the stiffness of the material in both filaments and 3D printed specimen; however, a different fracture behavior was observed due to the peculiar structure of printed samples.

Graphical abstract

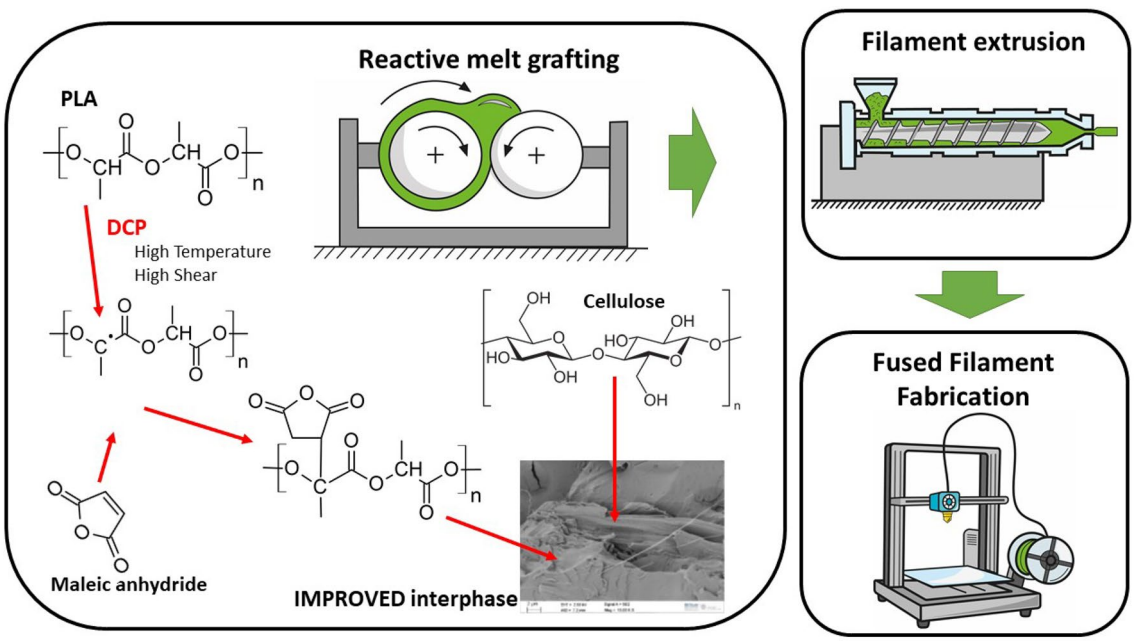

Keywords Poly(lactic acid) · Microcellulose · Fused filament fabrication · Maleic anhydride

Extended author information available on the last page of the article

1 Introduction

Fused filament fabrication (FFF) is one of the more attractive additive manufacturing (AM) techniques due to the continuous decrease of the related costs, high speed and simplicity of the process [1]. The advantages of FFF over conventional manufacturing processes are the possibility of free design and the absence of a mold in manufacturing thus allowing the construction of complex parts at low costs [2]. FFF is a method to build up objects layer by layer with the support of computer aided design. A filament is heated inside a nozzle, mounted on a moving system and then extruded in a controlled manner from the bottom layer to the top layer to form the final object [3]. At present, various materials are available for FFF ranging from thermoplastic polymers, such as polyamide [4], high-density polyethylene [5], acrylonitrile butadiene styrene (ABS) [6], polylactic acid (PLA), polyetherimide (PEI) [7], thermoplastic polyurethane [8] and polyvinyl alcohol (PVA) [9], to ceramic [10], gypsum, metals, food [11] and even concrete [12]. Polymers based on lactic acid (PLA) are one of the most promising type of plastic materials made from renewable resources due to their good mechanical properties, excellent workability, great barrier properties [1] and biodegradability [13, 14]. PLA is a compostable polymer obtained from renewable resources; it has been viewed as a good contender to reduce the societal solid waste disposal problem. Its low toxicity, along with its environmentally green properties, could make PLA an ideal material for food packaging and for other consumer goods. Nevertheless, some weak points mainly represented by its low ductility, poor toughness, low glass transition temperature, high sensitivity to moisture and relatively low gas barrier should be solved [15, 16]. The use of natural or synthetic fibers is well investigated to obtain specific characteristics and major increases of the properties of polymeric matrices [17]. Natural materials added to a PLA matrix act mostly as a filler to decrease costs without losing the green benefits of a biopolymer [18] or to improve the biodegradability [19]. The combination of natural fillers, characterized by a hydrophilic behavior, into hydrophobic thermoplastic polymers typically results in weak dispersion, high viscosity, and poor compatibility. The weak interfacial adhesion between the filler and the matrix usually leads to composites with inferior mechanical properties [20]. Compatibilizers are commonly applied to enhance the interface between the fillers dispersed in the polymer matrix. Maleic anhydride (MAH) does not homopolymerize under the reaction conditions used in grafting reactions which makes it a good compatibilizing material. Free radical melt grafting of maleic anhydride on the polymer chains of polyolefins is an efficient and simple way to enhance the compatibility of polymer and different kind of natural fiber from micro- to nanometric scale. Several studies of free-radical grafting of MAH different polyolefins, such as: LDPE, HDPE, PP, EPR, EPDM are described in literature [21]. This reaction is commonly accomplished when the molten polymer is mixed with MAH and with a peroxide initiator, either in an extruder or in an internal mixer. Grafting was successfully performed in an internal mixer at temperature of 190 °C and 60 RPM on PLA, where dicumyl peroxide was utilized as initiator at concentration between 0.1 and 0.2 wt% and MAH added at concentration between 0.3 and 3 wt% [22, 23]. A grafting amount of 0.2–0.5% was defined by titration analysis, depending on the content of MAH. A concentration of dicumyl peroxide of 1 wt% resulted to be an ideal preparation to maximize the grafting process and minimize the possibility of undesired side reactions [24, 25]. Moreover, it was highlighted that a maleic anhydride content higher than 5 wt% led to non-significant improvements [26]. Organic clays such as montmorillonite [23], bentonite and hectorite [27] are employed to enhance the mechanical properties of composite. Frequently, a proper compatibilizer is added to PLA to encourage a better dispersion of non-polar organoclay. Maleic anhydride is a common choice to manufacture high values composites starting from PLA and agricultural wastes. For example, rice husk was an attractive chance due to its low cost, renewability, biodegradability and low density. Tsou et al. [28] suggested a possible way to recycle it and combine this waste material in PLA to make green composites through the modification of PLA via reaction grafting in the melting state with MAH. Zhu et al. [29] performed a wide study on the opportunity to use soy protein, an agricultural residue of the soybean oil crushing, as a filler to be compounded with PLA grafted MAH to decrease the total cost while increasing the degradation rate of the composites. The hydrophilic functionalization with maleic anhydride was examined to enhance the compatibility between PLA and wheat straw by Nyambo et al. [30]. Both PLA and starch are brittle elements and lack of chemical compatibility, this results in a brittle composite with low strength, which could be enhanced by introducing MAH as a compatibilizer as demonstrated by Zhang et al. [31]. They demonstrated that the mechanical properties of PLA/starch composites are enhanced with just 1 wt% of MAH. In fact, PLA/starch (55/45) composite achieved a tensile strength of 52.4 MPa, 20% more that the materials without MAH and similar to the neat PLA. Micro cellulose and nanocellulose have been encouraging assessed as reinforcing filler for various composites [32]. Specific composition in PLA have been made either by solution casting up to 20% of nanocellulose [33], or by melt compounding with 5% of nanocellulose crystals [34] and with 1% of microcrystalline cellulose [35]. Moreover, some researchers recently proposed the use of cellulose based composite for 3D printing [9, 36]. PLA has been utilized to prepare bio-based and biodegradable

composites filled with cellulosic materials to decrease the overall costs and enhance the mechanical properties [37, 38].

The aim of this work is to study the addition of microcrystalline cellulose into PLA matrix through the grafting of maleic anhydride (MAH) on the PLA backbone as a compatibilizing agent. Filaments composite with increasing amount of MCC are 3D printed with a desktop FFF machine. The mechanical properties, thermal stability and morphology of the resulting composites are characterized and the synergetic effects of the compatibilization and MCC on the mechanical behavior of the composites are evaluated.

2 Materials and methods

2.1 Materials

Poly(lactic acid) (PLA) grade 4032D with density of 1.24 g cm^{-3} and a melting point of 155–170 °C was provided by Nature Works LLC (Minnesota, USA). PLA 4032D is an ideal product for laminations and other packaging applications, due to the excellent optics, good machinability and excellent twist and dead fold. Microcrystalline cellulose, MCC, (specific gravity = 1.56 g cm^{-3}, mean molecular weight = 90,000 g mol^{-1}) prepared through the reaction of cellulose with a water solution of strong mineral acid at boiling temperature, supplied by Sigma Aldrich (USA), were selected as microscale reinforcing filler. MCC particles consist of elongated flakes with an average length of about 24 µm and a diameter of about 10 µm measured with the aid of an optical microscope. Maleic anhydride (MAH) and dicumyl peroxide (DCP) were provided by Sigma Aldrich (USA).

2.2 Compounding and melt-grafting

Both PLA pellets and microcrystalline cellulose powder were dried in a ventilated oven at 50 °C for 24 h before being processed. PLA with various amounts of microcrystalline cellulose were melt-compounded with or without compatibilizer (PLAgMAH) in a *Thermo Haake* internal mixer at a temperature of 165 °C, with a revolution speed of the rotors of 60 rpm and a processing time of 15 min.

Grafting of maleic anhydride (MAH) on the backbone of PLA (PLAgMAH) was performed via radical grafting directly during the melt compounding process with the presence of dicumyl peroxide (DCP) as a radical initiator, following a procedure well described in literature [22]. The PLA was melted for 2 min and then DCP and MAH were added at a ratio of 1:10 DCP/MAH and mixed for 3 min. The reaction with MAH in quantities from 1 wt% to 10 wt% continued during mixing for 5 min. Eventually, MCC was added and mixed for another 5 min. At the end various, batches of PLA/MMC and PLA/PLAgMAH/MCC were cooled down and grinded at room temperature by IKA grinder M20 Universal mill.

According literature [22], the first step of grafting is the formation of primary radicals via the decomposition of dicumyl peroxide, which then initiates PLA macroradicals by a hydrogen extraction mechanism. The macroradicals subsequently react with maleic anhydride. A possible mechanism of grafting MAH on PLA is schematized in Fig. 1.

2.3 Filaments extrusion

PLA compounded with 10 wt% of MCC, and PLA grafted with 1 wt% of MAH compounded with 10 wt% of MCC were grinded and used as masterbatch material to be mixed with neat PLA powder to reach the desired microcellulose concentration in the filaments. The filaments were obtained using a Next 1.0 (3Devo, Netherlands) single screw extruder. It was characterized by a nozzle of 3 mm in diameter and an optical encoder to measure the diameter of the extruded filament that allowed an automatic adjustment of the drawing speed to maintain a stable diameter. With this feature, an average diameter of 1.75 ± 0.04 mm was obtained. A

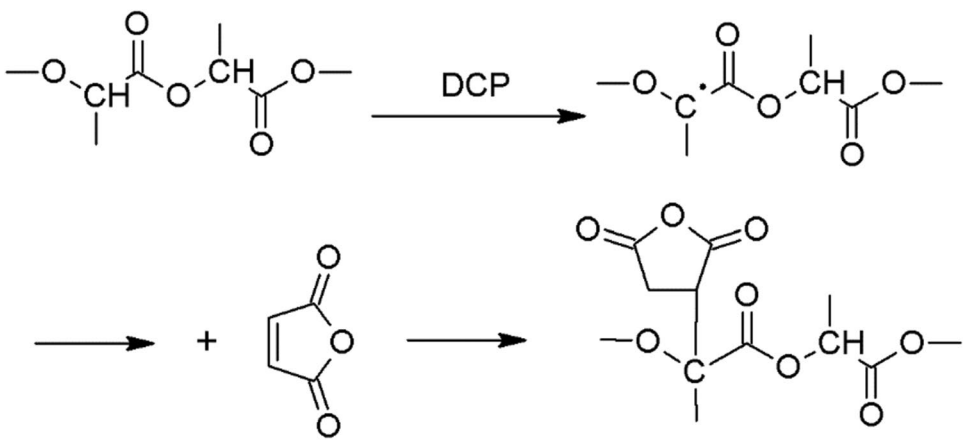

Fig. 1 Possible mechanism of grafting MAH on PLA

temperature profile of 170 °C, 190 °C, 185 °C and 175 °C in the die zone and a rotation speed of 5 RPM were chosen. Neat PLA, PLA compounded with MCC and PLA grafted MAH compounded with MCC filaments containing from 1 wt% to 10 wt% of microcellulose were produced via extrusion. Produced compositions are reported in Table 1.

2.4 Fused filament fabrication

Sharebot Next Generation desktop 3D printer (Sharebot NG) with a nozzle diameter of 0.35 mm was used for the fabrication of dumbbell specimens according to ISO527 1BA standard (Fig. 2a). A digital 3D model of the samples was built with the aid of the software SolidWorks® and it was exported in STL format. Through the freeware software Slic3r in Fig. 2b, a G-code file was compiled with the following parameter for the printing: rectilinear type of infill, infill angle ±45°, infill percentage 100%, no raft, layer height 0.2 mm, nozzle temperature 220 °C, bed temperature 40 °C and deposition rate 40 mm/s.

Interlayer adhesion of FDM compact tension (CT) specimens was investigated through the evaluation of fracture toughness according to ASTM D5045. Their dimensions were 24 mm (W) × 24 mm (H) × 5 mm (T), with a crack length of 6 mm as shown in Fig. 2c. CT specimens were printed with the same parameters reported before to have the crack plane aligned with the layers as visible in Fig. 2d. In each specimen, a sharp notch of 9 mm in length was done by means of a broaching machine equipped with a fresh razor blade (Fig. 2e). Specimen were tested in tensile configuration with a self-made interface between specimen and tensile machine visible in Fig. 2f.

2.5 Testing techniques

The grafting reaction of maleic anhydride on PLA was investigated through Fourier-transform infrared spectroscopy (FTIR) analysis carried out by a Spectrum One from Perkin–Elmer in ATR configuration. Spectra were collected in the wavenumber range from 4000 to 650 cm^{-1} by averaging 4 scans.

Degradative mechanisms of the materials while subjected to a constant heating were studied with thermogravimetric analysis (TGA). The analysis was performed using a TA Instruments TGAQ5000IR machine, with a heating rate of 10 °C/min in the range between 40 °C and 700 °C flushing nitrogen at 15 ml/min.

Viscosity was also measured as a function of shear rate using an Anton Paar MCR 301 rheometer. Before experiments, the samples were dried at 40 °C for 24 h. The rheometer was operated in the rotational mode with parallel plate geometry at 190 °C, over a shear rate range of 10 to 1000 s^{-1}. Before testing, the samples were kept under vacuum at room temperature for 24 h to remove completely the humidity.

Density of the 3D printable filaments was measured with an Archimedes balance in double distilled water at room temperature through a Gibertini E42 analytical balance following ASTM D792 standard.

Microstructural observations of cryo-fractured surfaces of the 3D printed specimens were performed with a Zeiss Supra 40 high resolution field emission scanning electron microscope (FESEM) with an accelerating voltage of 2.5 kV. Sample were coated with a thin platinum–palladium conductive layer.

Differential scanning calorimetry (DSC) was performed with a Mettler DSC 30 calorimeter. The tests were performed from 20 °C to 200 °C at a heating and cooling rate of 10 °C/min under a nitrogen flow of 100 ml/min. Glass transition temperature T_g, crystallization temperature T_c, melting temperature T_m and the degree of crystallinity χ_c were evaluated. The value of enthalpy for fully crystalline PLA was taken to be 93.6 J/g [39].

Dynamic mechanical thermal analysis (DMTA) tests were carried out using a TA Instrument DMA Q800 device, in the temperature range from −10 °C to 150 °C, at a heating rate of 3 °C/min, a strain amplitude of 0.05% and a frequency of 1 Hz. The storage modulus (E′), the loss modulus (E″) and

Table 1 Sample code and final composition of filaments and 3D printed parts

Code	PLA (wt%)	MCC (wt%)	MAH (wt%)	DCP (wt%)
PLA	100	0	0	0
PLA_01MCC	99	1	0	0
PLAgMAH_01MCC	98.89	1	0.1	0.01
PLA_03MCC	97	3	0	0
PLAgMAH_03MCC	96.67	3	0.3	0.03
PLA_05MCC	95	5	0	0
PLAgMAH_05MCC	94.45	5	0.5	0.05
PLA_10MCC	90	10	0	0
PLAgMAH_10MCC	88.9	10	1.0	0.10

the loss tangent (tan δ) were evaluated as a function of the temperature.

Quasi-static tensile tests were performed using an Instron 5969 tensile test machine, equipped with a 50 kN load cell at room temperature with a crosshead speed of 10 mm/min. At least five 3D printed dumbbell specimens shape 1BA according to ISO527 standard for each composition were tested.

Fracture toughness of the interface between two subsequent layers was determined through a tensile test on CT specimen at 10 mm/min according to ASTM D5045 evaluating the stress intensity factor to measure the stress field around the crack tip with Eq. 1:

$$K_Q = \frac{P_Q}{BW^{1/2}} f(x) \tag{1}$$

K_Q is a conditional fracture toughness calculation, P_Q is a conditional load identified according to ASTM D5045, B is specimen thickness, W is specimen width, a is the crack length, x is the crack length to specimen width ratio a/W ($0.2 < x < 0.8$) and f(x) is tabulated in ASTM D5045. To validate the linear elastic plane-strain fracture toughness measurement, P_Q is determined by finding the intersection of the load vs. crack opening curve and a line having a compliance 5% greater than the initial slope of the curve. P_{max} is then taken to be the maximum load sustained by the specimen. Under the following conditions, K_Q is equivalent to K_{IC}:

$$\frac{P_{MAX}}{P_Q} < 1.1 \tag{2}$$

$$B, a, (W - a) > 2.5 \left(\frac{K_Q}{\sigma_y} \right)^2 \tag{3}$$

where σ_y is the yield strength of PLA, which is taken to be 55 MPa based upon previous material testing.

The results of mechanical tests were evaluated using ANOVA with the software R-Cran, considering the quantity of MCC, MAH and their interaction. The P value was used as a tool to check the significance of the examined variables. A P value lower than 0.05 (i.e., 95% confidence interval) indicates that the examined parameter is significant.

The samples coding based on the composition is summarized in Table 1. For example, a sample coded PLAgMAH_05MCC indicates the presence of 5 wt% of MCC in a matrix composed of PLA grafted with MAH. According to the preparative methods previously described, the content of MAH is fixed at 10 wt% of MCC, and DCP is 10 wt% of MAH.

3 Results and discussion

FTIR is an effective technique to analyze the structures of maleated polymers. In fact, the presence of MAH grafted on PLA backbone can be identified by comparing the FTIR spectra of PLA filaments extruded with and without MAH and DCP (see Fig. 3). The whole spectra are shown in Fig. 3a, while in Fig. 3b, c, a focus on the peaks related with the grafting of MAH is detailed. Comparing the spectra of neat PLA and the ones of PLA grafted with maleic anhydride, it is possible to observe the presence of new absorption band, in particular at: 695 cm^{-1} corresponding to the bending of vinyl C–H in MAH that could be referred to the presence of non-grafted MAH [22, 40]; 820 cm^{-1} corresponding to the out of plane deformation for carboxyl groups from MAH [41]; 1635 cm^{-1} corresponding to the cyclic C–C stretching that might be a confirmation of the chemical interaction between PLA and MAH [26, 41]; 1790 cm^{-1} (appearing as a shoulder due to the overlapping with the very large peak of the carbonyl >C=O stretching of PLA at around 1748 cm^{-1}) and 1850 cm^{-1} are assigned to the symmetric and asymmetric stretching of the carbonyl groups of the saturated cyclic anhydride ring of MAH, respectively [22, 24, 26, 42]. The absorption peaks are clearly visible only for PLAgMAH10, due to the highest amount of MAH, differently from the other two samples with low MAH content (1 wt% and 5 wt%) [42]. FTIR spectra of MCC composites confirmed the presence of the same correspondent peaks of PLA or maleated PLAs (plots not shown).

Thermal degradation behavior of the micro composite materials was investigated through thermogravimetric analysis on filaments specimens and the thermograms are reported in Fig. 4.

In particular, as reported in Fig. 4a, neat PLA is characterized by a single degradation step centered at 370 °C. The onset decomposition temperature of neat PLA is found to be around 315 °C. The decomposition temperature of the samples was affected by the addition of MAH. Moreover, the weight loss started at around 290 °C for MAH grafted samples, and this could be correlated with the lower molecular weight of PLA when it is MAH treated [22]. An initial weight loss, between 0.5% and 1%, was found for all the filaments and, according to the derivative curve peak at 100 °C, this could be related to the evaporation of residual water. For samples with the highest amount of MCC, a small peak in the derivative thermogravimetric curves was detected at around 160 °C. This peak could correspond to the degradation of the small oligomeric chains formed during the melt compounding process.

Viscosity is a key parameter in extrusion-based AM systems in which the polymer must be first transformed in a filament which is then melted inside a nozzle prior to be

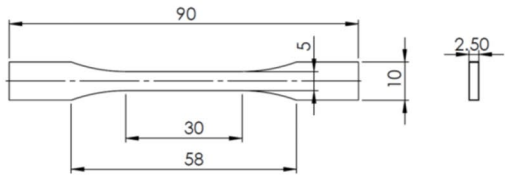

(a)

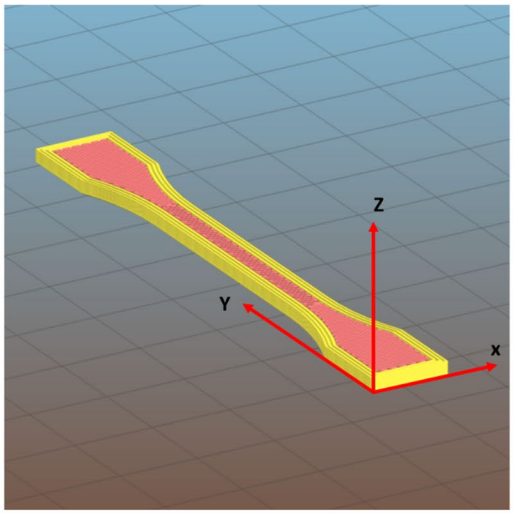

(b)

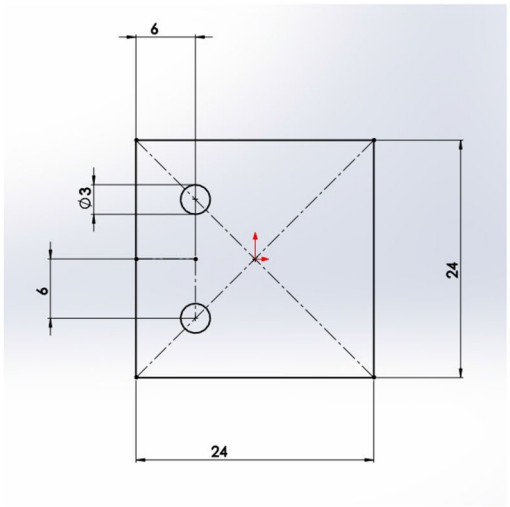

(c)

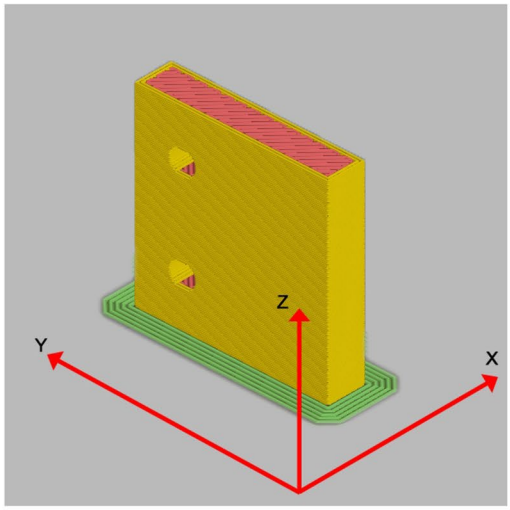

(d)

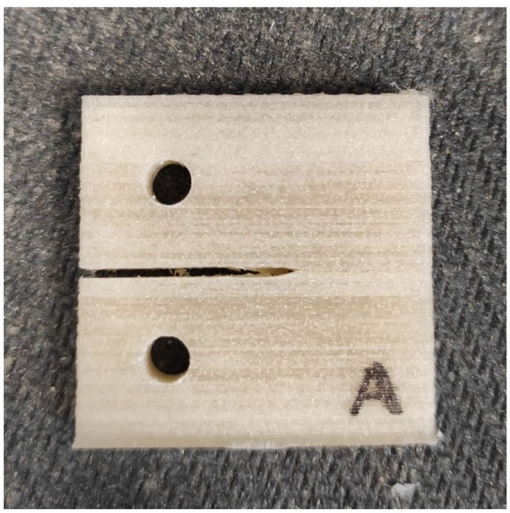

(e)

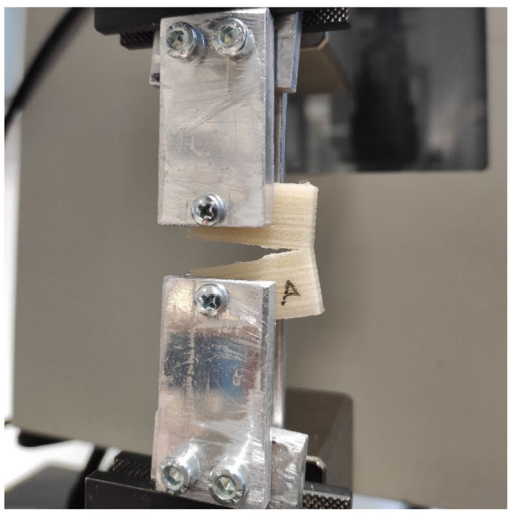

(f)

◂**Fig. 2** **a** Dimension of ISO527 1BA specimen (all the measurements are in mm), **b** 3D draw of dumbbell specimen upon slicing **c** Graphical picture of the CT specimen as draw in SolidWorks (all the measurements are in mm), **d** 3D draw of the specimen during printing, **e** CT specimen after notching and **f** tensile test

deposited on the building plate to form the desired object. The addition of MCC slightly decreased the viscosity of biocomposites up to 3% of microcrystal cellulose with or without PLAgMAH. It is also worth noting the synergistic effect of MAH on viscosity of composites at 5% and especially at 10% of MCC. Furthermore, a broader view of the combined effect of MCC and MAH on the apparent viscosity as a function of the shear rate can be correspondingly appreciated in Fig. 5.

Biocomposites at 1% and 3% of MCC behaved similarly to PLA at low shear rate but exhibited higher viscosity at higher shear rate. On the other hand, a significant and progressive reduction of viscosity could be observed for compositions above 3wt% of MCC, in PLA and PLAgMAH, and the decrease appeared more rapid for samples with MAH at low shear rate. This behavior could be attributed to the presence of micrometric fillers with a low area over volume ratio and due to the poor interaction between MCC and neat PLA for samples without MAH. Despite the improved interaction between PLA and MCC given by MAH, viscosity of biocomposites at 5% and 10% of MCC decreased furtherly, due to a possible decrease in molecular weight of PLA after the reaction with DCP that hinders the improved matrix–filler compatibility, in particular for, as reported in similar studies [22, 24]. The shift of the viscosity curves towards lower values and the fading of the shear-thinning behavior could be correlated with a decrease in the molecular weight as reported by Cooper-White et al. [43] for PLLA with decreasing molecular weights. A similar behavior was observed by Barczewski et al. [44], in fact they found an increase in MFI of PLA biocomposites with the increasing content of lignocellulosic filler, i.e., micrometric grinded nutshell.

Figure 4 shows a shear thinning behavior for neat PLA and microcomposite materials without MAH above 100 s^{-1}. Shear rates in the nozzle of a FFF machine are commonly in the range of 100–200 s^{-1} [45], so the decrease in viscosity played by the incorporation of MCC and the shear thinning behavior around 100 s^{-1} appeared beneficial effects for the printability of these biocomposite filaments. On the other hand, the compounding of MCC with PLAgMAH determined a significant reduction of viscosity at low shear rate, but in the processing zone at about 200 s^{-1} the slight increase of viscosity was not considered critical for 3D printing. In the case of PLAgMAH_10MCC the effect of viscosity decreased due to DCP seemed to be compensated by the addition of MCC in almost all the range of shear rate.

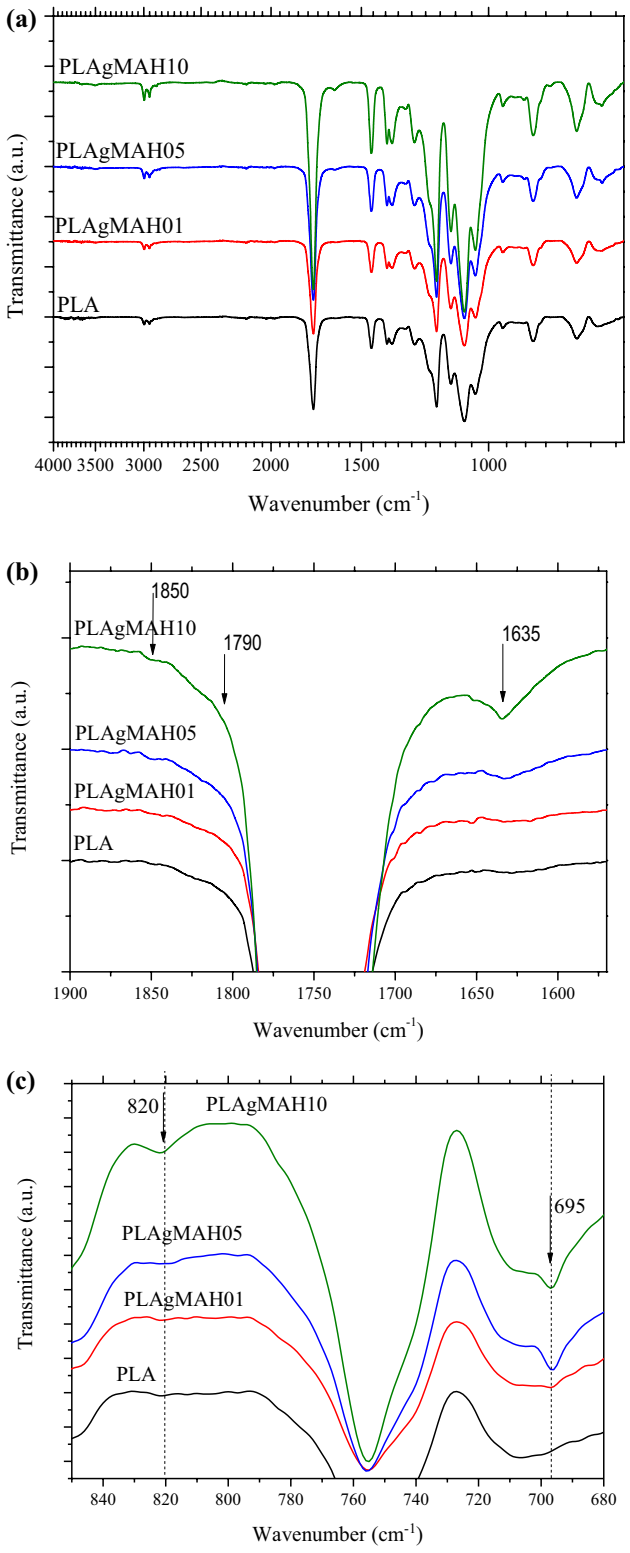

Fig. 3 **a** FTIR spectra for neat PLA and selected PLA grafted MAH and **b**, **c** focus on the peaks related with the grafting of MAH

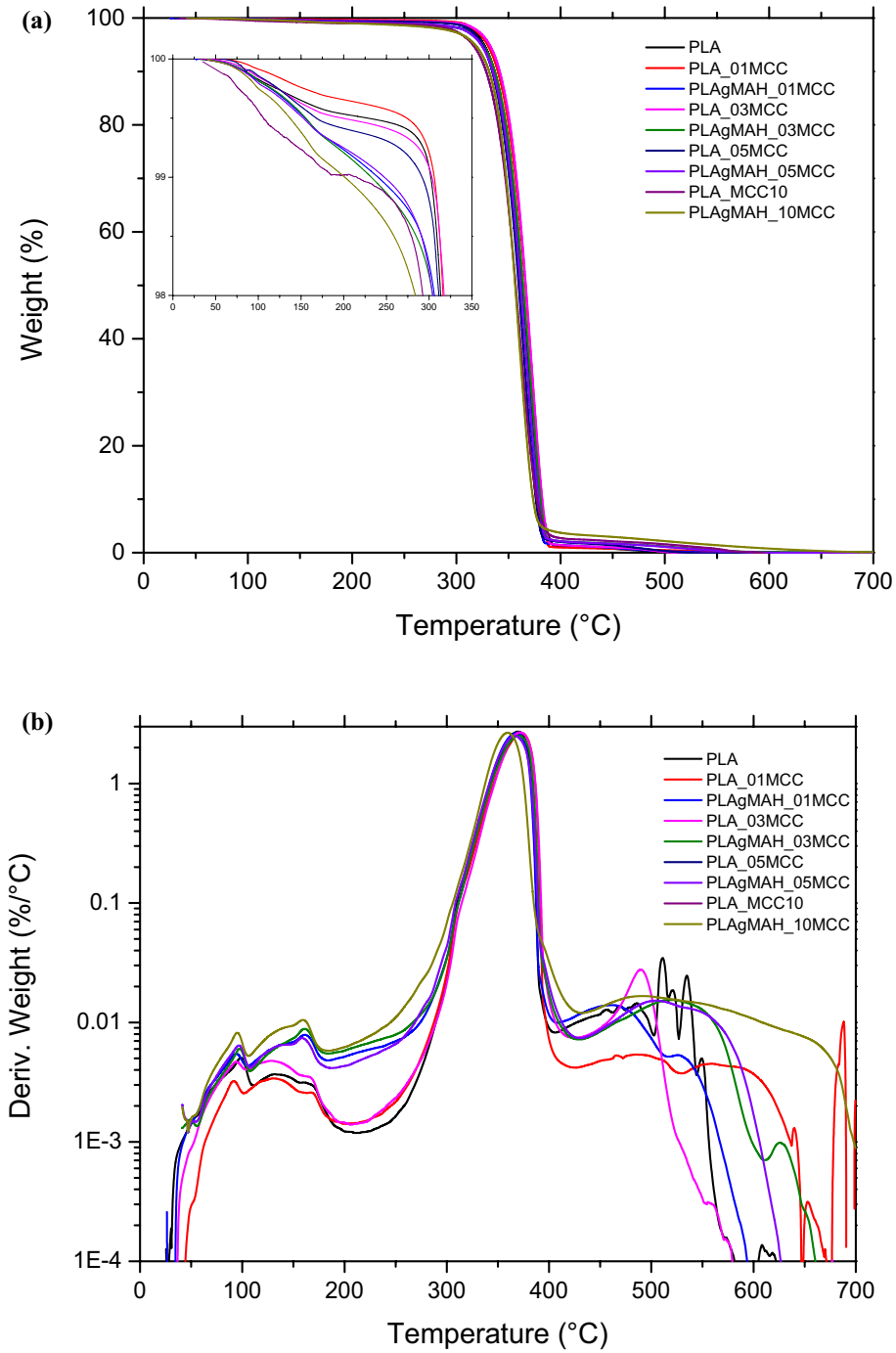

Fig. 4 Thermogravimetric curves (**a**) and derivative curves (**b**) of neat PLA compared with PLA grafted MAH with different amount of MAH and MCC

Thermal properties of the PLA, PLA/MCC and PLA grafted MAH/MCC composite filaments were determined using differential scanning calorimetry (DSC) and the thermograms are reported in Fig. 6. The glass transition temperature, the crystallization and melting temperatures, the crystallization and melting enthalpies and degree of crystallinity obtained from the DSC are reported in Table 2. Glass transition is a complex property which is related to several factors including intermolecular interactions, steric effects, chain flexibility, molecular weight, branching and cross-linking density. Due to the poor compatibility between cellulose and PLA, glass transition is not expected to change upon the introduction of MCC [46, 47], but Tg could decrease by the presence of maleic anhydride grafted on PLA, due to an increased mobility of the polymeric chains [42]. The improved chain mobility promoted by MAH and the nucleating effect of MCC lowered the crystallization temperature [48]. Crystallization temperature (T_c) and crystallinity fraction (X_c) are affected by the introduction of microcellulose and maleic anhydride. Maleic anhydride increases

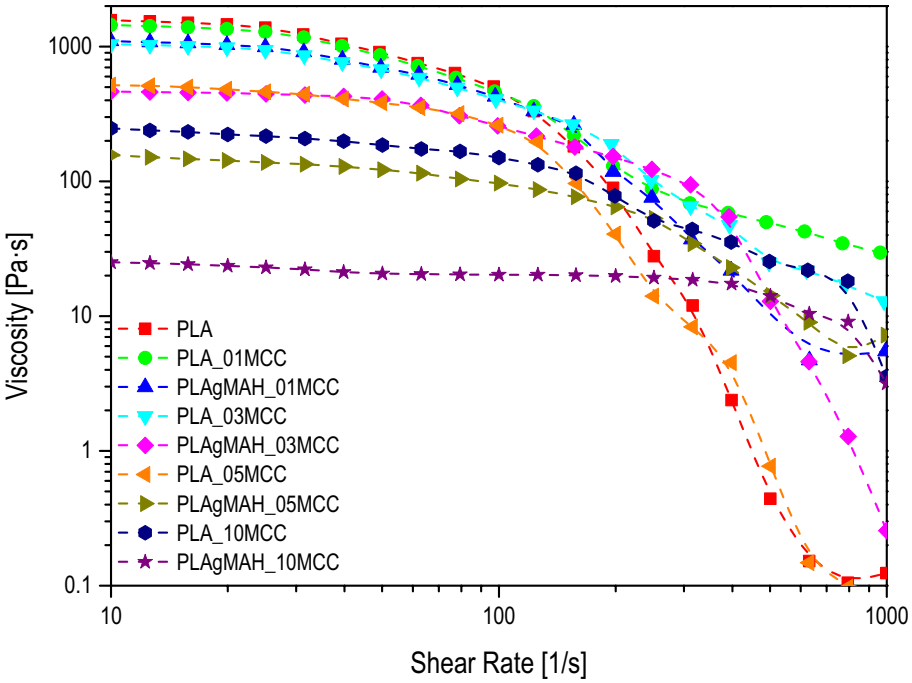

Fig. 5 Viscosity values for filaments made of PLA and PLA grafted MAH as a function of the content of MCC

the crystallinity fraction with respect to the corresponding PLA–MCC composite filament. The melting temperature of neat PLA crystallites is identified at around 168 °C and slightly increased with the presence of filler. From this increase in melting temperature, MCC appeared to affect the crystalline structure of PLA in terms of size and perfection of the crystalline lamellae of PLA [49]. The maximum amount of crystallization, according to the crystallization enthalpy (ΔH_c), is observed for the sample loaded with 1, 3 and 5 wt% of MCC in the presence of MAH. This confirms the previous observations related to the role of cellulose as nucleating agents for PLA [47, 50]. The maximum of crystallizability X_{max} could be calculated by the enthalpy of melting peak, as reported in table, and it showed an increase from about 26% of pristine PLA, to about 39–45% for MCC biocomposite. The higher the content of MCC, the higher the crystallizability, and even higher in the presence of PLAgMAH.

Storage modulus curves of 3D printed specimen as a function of temperature are shown in Fig. 7a. In the glassy zone below the glass transition temperature, PLA exhibits its value of E′ (about 1300 MPa at 23 °C) lower than that of biocomposite. In particular, the addition of micro cellulose pushes E′ towards 1450 MPa at 23 °C in the case of PLA_10MCC. The grafting of maleic anhydride boosts the stiffening effect of MCC for all the composition, and the value of E′ at 23 °C of PLAgMAH_10MCC reaches 1480 MPa. At temperatures that correspond to the glass transition temperature as revealed by DSC, it is possible to observe a drop in the E′ value that seems to match the decrease in T_g found in DSC for as concerns the shift of this drop towards lower temperature. Above 100 °C storage modulus starts to increase again due to crystallization process and also in this case the curves are shifted to left with an increased amount of micro-cellulose due to a possible nucleating effect or a more favorable chain mobility promoted by the viscosity decrease. Figure 7b shows loss factor (tan δ) curves as a function of temperature for 3D printed specimen. Neat PLA exhibits the lowest damping peak (2.07 at 74 °C) between all the tested composition, but no trend can be evidenced with the increase of MCC or with the presence of MAH. However, all the peaks related to micro-composite material are higher than the one of neat PLA, resulting in the range 2.2–2.6. This effect highlights a slightly better damping performance when micro-cellulose is added to the PLA matrix.

Mechanical properties from quasi-static tensile test on filaments and 3D printed specimen are summarized in Figs. 8, 9respectively. MCC was found to significantly (p value $= 2.1 \times 10^{-6}$) increase the elastic modulus of 3D printable filaments. Maleic anhydride had a lower effect on elastic modulus (p value $= 0.014$), it is possible to appreciate a higher stiffening effect with an increasing amount of MCC for the samples loaded with MAH (Fig. 8a, b). This effect could be explained by an improved interface between the MMC filler and the PLA matrix, but also by a slight increase in the crystallinity of the material as previously seen in DSC and due to a plasticizing effect of MAH. However, this stiffening effect was not translated to 3D printed samples, where no effect of MCC was appreciable (Fig. 9a, b). The variation

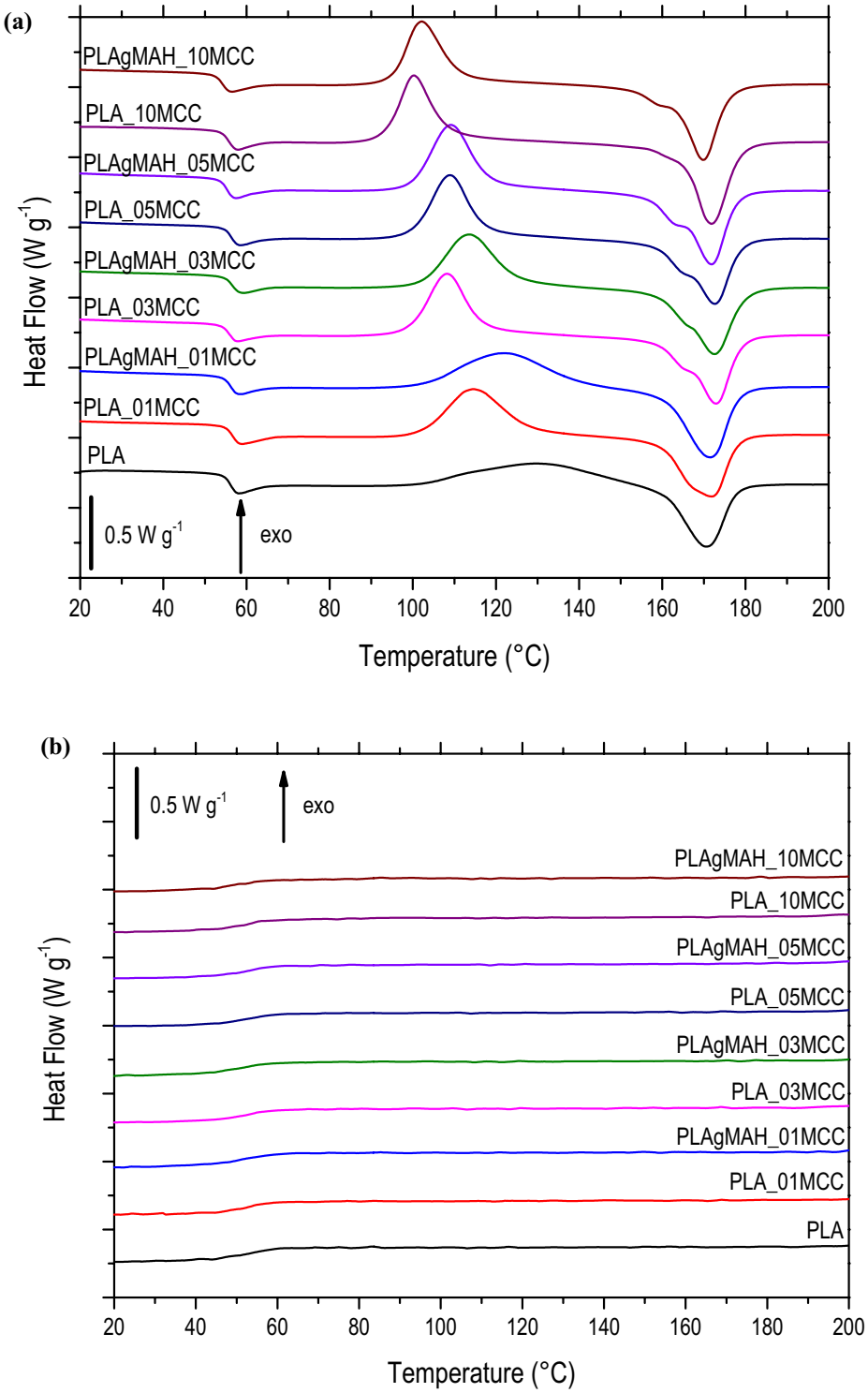

Fig. 6 Representative DSC curves for filaments made of PLA/MCC and PLA grafted MAH and MCC, first heating (**a**) and cooling (**b**) scan

in the elastic modulus of 3D printed samples, as highlighted by ANOVA, is slightly affected by the interaction between MCC and MAH (p value = 0.062). The statistically significative difference between 3D printed samples made of PLA grafted or not with MAH could be due to the increase of the crystallinity fraction or by the enhanced printability and so the density of the specimen.

In fact, it is important to state that the increasing the amount of micro cellulose inside the PLA could impair the printability of these composite due to the clogging of the nozzle during printing and so the easiness to print [36].

Table 2 Crystallinity degree according to first scan and glass transition temperature (T_g), crystallization temperature (T_c), melting temperature (T_m) and transition enthalpy for PLA and relative microcomposite filaments from DSC curves

	X_c (%)	T_g (°C)	T_c (°C)	ΔH_c (J g^{-1})	T_m (°C)	ΔH_m (J g^{-1})	X_{max}* (%)
PLA	1.1	59.2	134.0	23.0	168.0	24.0	25.6
PLA_01MCC	1.7	59.4	120.5	34.2	167.2	35.8	38.6
PLAgMAH_01MCC	0.6	59.5	128.1	36.8	168.5	37.4	40.4
PLA_03MCC	0.9	59.5	113.4	35.4	170.4	36.2	39.9
PLAgMAH_03MCC	0.2	59.2	117.2	37.1	170.4	37.3	41.2
PLA_05MCC	1.1	59.1	113.6	34.6	170.3	35.6	40.0
PLAgMAH_05MCC	2.0	58.6	113.2	37.0	169.5	38.8	43.9
PLA_10MCC	3.0	59.0	108.2	32.3	169.7	34.8	41.3
PLAgMAH_10MCC	3.1	57.3	108.2	34.4	167.8	37.0	44.5

*Max crystallizability (X_{max}) is calculated from the melting peak

Stress at break for filaments was negatively influenced by the presence of both MCC and MAH (Fig. 8c, d). MCC inside the polymer matrix acts as a geometrical defect, where the stress could become significantly greater than the surrounding region and leading to a premature failure of the component. A low p value ($<2.2\times10^{-16}$) for as concern the interaction between MAH and MCC indicates that MAH act as a weak and brittle interphase between PLA and MCC. This was particularly evident for the sample with the higher amount of MCC and MAH (PLAgMAH_10MCC). MCC and MAH are found to negatively affect the strain at break of the filaments (Fig. 8e, f). The embrittlement of composite material based on PLA with the introduction of MCC is in accordance with other studies in literature [19, 51]. The different structure of FFF specimen respects to a single filament led to different fracture mechanisms. It is possible to state that the energy at break could not consumed just by the fracture of the single strands that compose the objects but also by the debonding processes intra- and inter-layers [9]. A noticeable effect was found for the filler (p value = 0.019); however, the main reinforcing effect was given by the interaction of MCC and MAH (p value = 7.4×10^{-4}). Stress at break increased from 31.2 ± 5.1 MPa of the sample printed with neat PLA to 40.7 ± 0.8 MPa of PLA grafted MAH with 5 wt% of MCC (Fig. 9c, d). According to rheological observations, the decrease in viscosity could have enhanced the adhesion of subsequent layers and adjacent strands. As seen for filament samples, it is possible to detect a decrease in strain at break with the increasing amount of MCC (p value = 3.1×10^{-11}) and this is particular evident when MAH was added due to its brittle behavior (p value = 0.03) (Fig. 9e, f).

The cryogenic fracture surfaces of compression molded specimen produced with PLA and PLA grafted MAH with 5 wt% of MCC are shown in Fig. 10. In Fig. 10a , a very weak interface between the neat polymer matrix and the micro-cellulose can be observed. This behavior could be attributed to a poor chemical interaction between the hydrophobic PLA and the hydrophilic cellulose. Maleic anhydride resulted to be very effective in improving the filler–matrix adhesion. In fact, as it can be appreciated in Fig. 10b, a positive enhancement is clearly evidenced with just a low amount (1wt%) of MAH grafted to the PLA.

The fracture surface of 3D printed specimen after tensile test with increasing amount of microcellulose with and without the presence of maleic anhydride grafted on the PLA backbone are shown in Fig. 11. It is possible to notice the different mechanical response to tensile stress with the increasing amount of filler dispersed in the matrix. Neat PLA and PLA with the lower amount of MCC (Fig. 11a, b) showed an extensive energy absorption with the decohesion of the filaments.

At the highest concentration of filler, 5 wt% and 10 wt% (Fig. 11c–f), the fracture surface become flatter without the evidence of a macroscopic breakage possibly due to the decrease in viscosity that favors viscous flow thus enhancing the inter- and intra-layer adhesion. Filaments broke transversally to the applied stress without detaching from each other. Also, for 3D printed samples without the presence of MAH, it is possible to remark a poor compatibility between cellulose and PLA that led to a presence of a large amount of porosity inside the 3D printed filaments.

The density of 3D printed specimen was always lower compared to that of bulk material due to the porosity originated during the printing process (see Table 3).

The apparent density, reported in Table 3, was calculated by the ratio between the weight of the specimen and its volume (Eq. 4).

$$\text{Apparent density} = \frac{\text{weight}}{\text{volume}} \tag{4}$$

The volume was approximately evaluated using the Eq. 5, where w is the width of the specimen, b is the width at center (5 mm) of the specimen model with an area A equals to 520 mm^2 and t is the thickness.

$$\text{Volume} = \left(\frac{w}{b}\right)^2 At \tag{5}$$

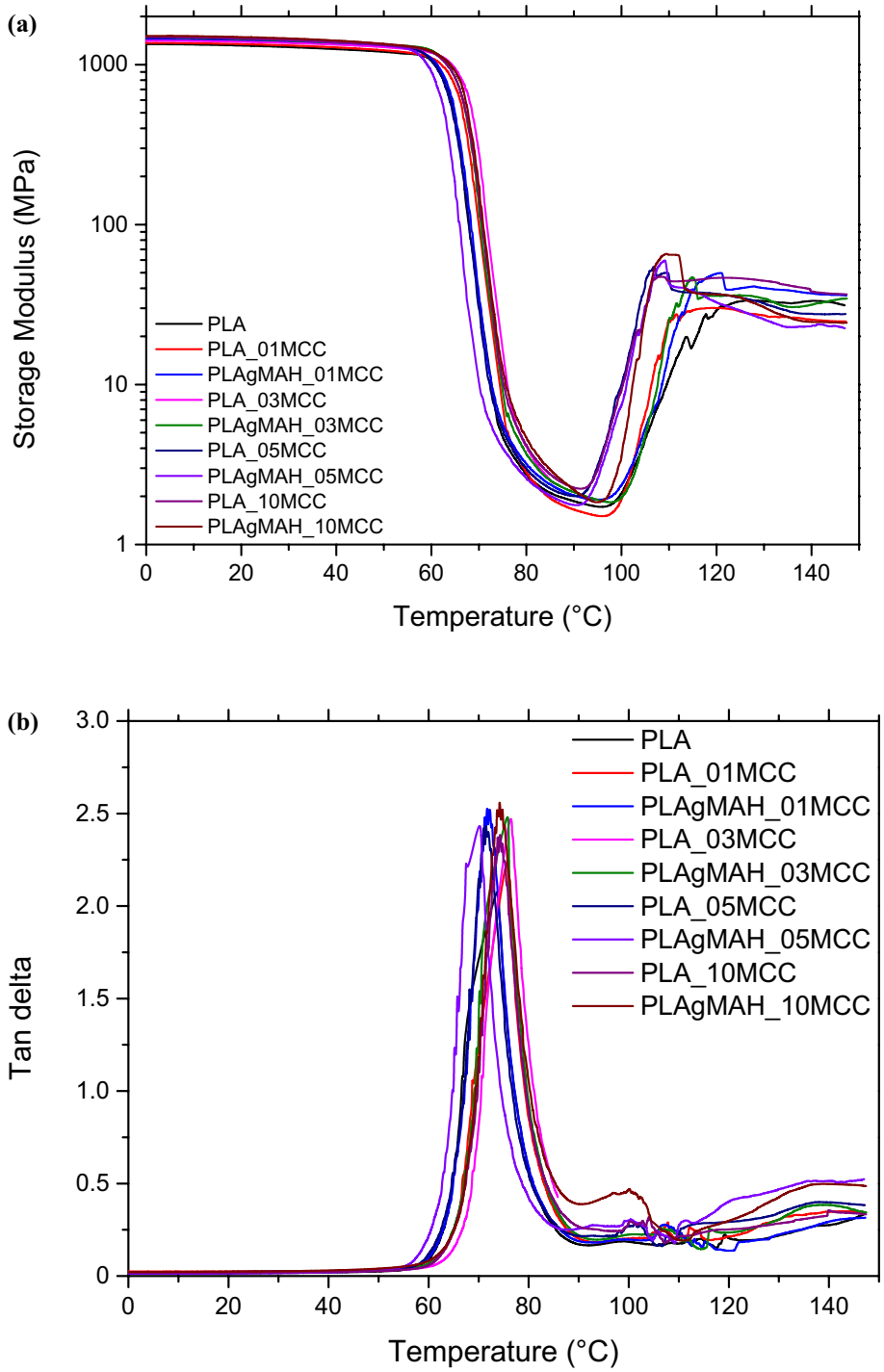

Fig. 7 Storage modulus (**a**) and tan delta (**b**) curves for 3D printed specimen of PLA and relative micro composite

The ratio between apparent density and the bulk density (Eq. 6), was calculated and it could be considered as an important parameter to estimate the mechanical properties of the material excluding the presence of voids and porosity.

$$R = \frac{\text{apparent density}}{\text{bulk density}} \tag{6}$$

The values of ratio R are reported in Fig. 12.

ANOVA showed no interaction between R and MCC; however, a significative effect was found for the interaction between R and MAH (p value = 0.034). This behavior could be explained by the pronounced decrease in viscosity due to the presence of MCC and MAH. It is important to underline that the tensile properties obtained from the mechanical tests on 3D printed materials reported in Fig. 8 do not take into

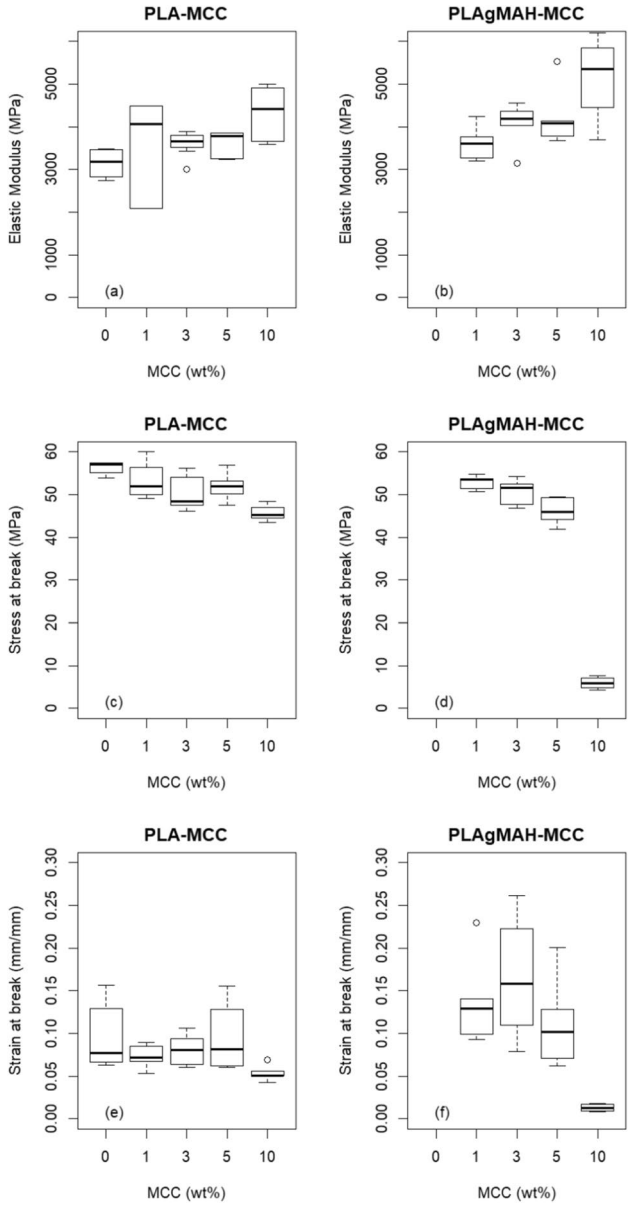

Fig. 8 Boxplot of the main mechanical properties related to micro-composite filaments as a function of wt% of MCC for PLA (**a**, **c**, **e**) and PLA grafted MAH (**b**, **d**, **f**)

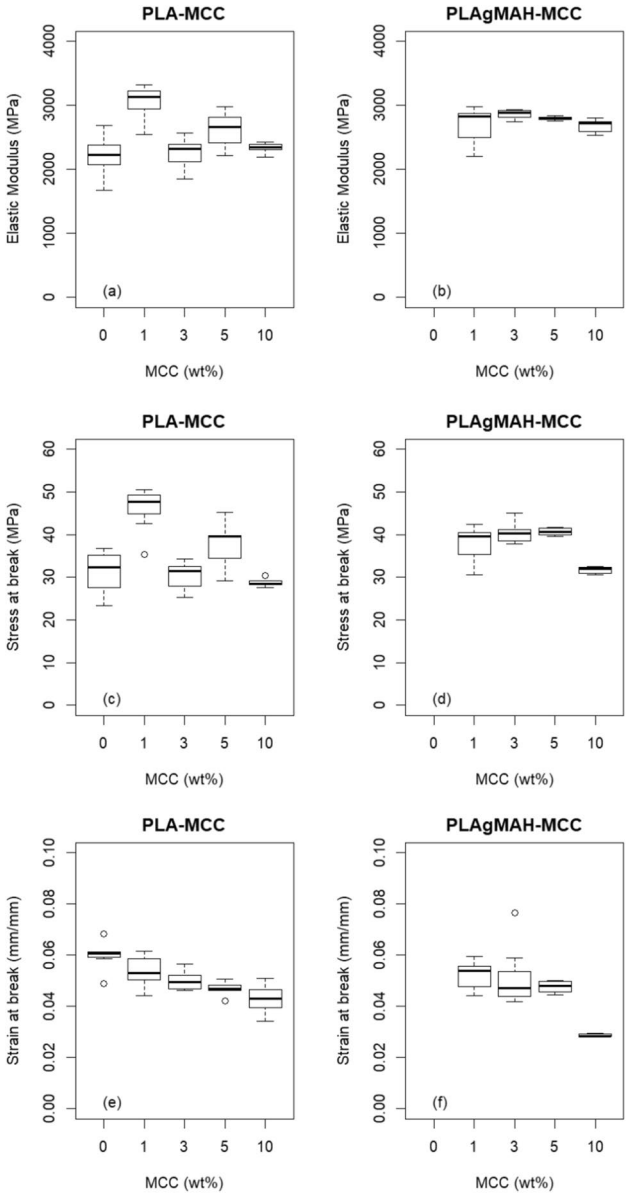

Fig. 9 Boxplot of the main mechanical properties related to 3D printed specimen as a function of wt% of MCC for PLA (**a**, **c**, **e**) and PLA grafted MAH (**b**, **d**, **f**)

account the presence of voids within the printed structure. It is, therefore, clear that the properties of 3D printed specimens resulted to be lower with respect to those obtained on the filaments from which were made. A statistical analysis was performed to correlate R with the mechanical properties of 3D printed specimen. A significative effect was found between elastic modulus and R (p value = 5.3e−5) and between stress at break and R (p value = 1.3e−3). These results are particularly true, since elastic modulus and stress at break are measured in relation of the cross section of the specimen and so of its volume. As proof of this, ANOVA showed no interaction between strain at break and R in the 95% confidence interval. Maximize the R ratio must be

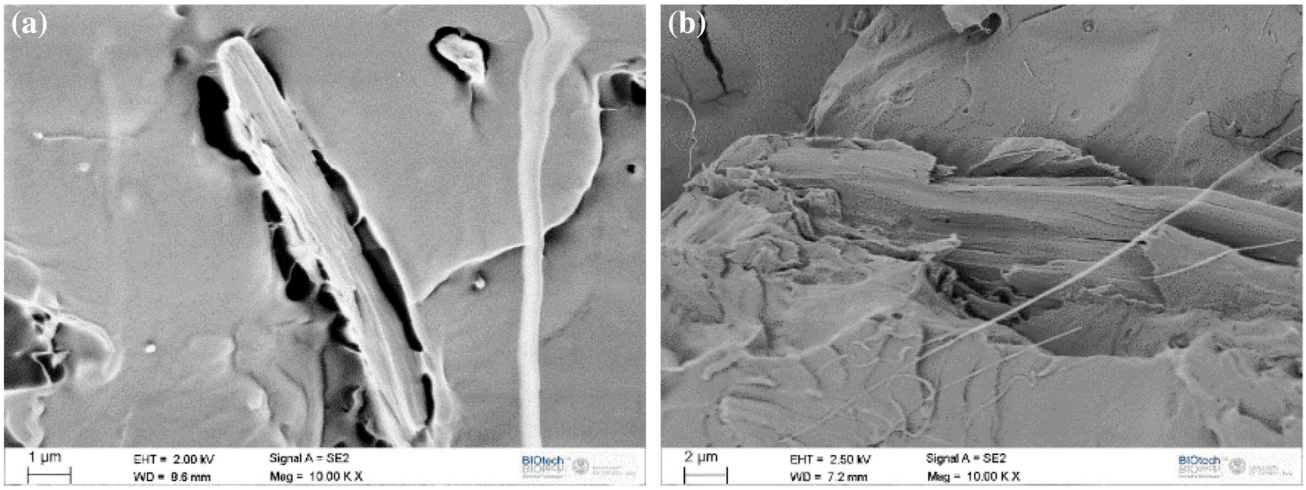

Fig. 10 SEM pictures of cryofractured surface of PLA_05MCC (**a**) and PLAgMAH_05MCC (**b**) compression molded sheets evidencing a good improvement of the interphase between microcellulose and PLA upon the melt grafting of maleic anhydride

a strategy to improve the stiffness and the strength of 3D printed objects.

The strength of the interface between two consecutive layers in 3D printed objects is affected by the bonding between the two layers and it is impaired by the presence of voids and defects [52]. Fracture toughness refers to a property which describes the ability of a material containing a crack to resist further fracture and it could be helpful to evaluate the interlaminar adhesion of additive manufactured objects [53, 54]. In Fig. 13 is graphically illustrated the behavior of the critical stress intensity factor against the concentration of MCC in presence or not of MAH. All the samples met the requirements for a linear elastic plane strain fracture toughness measurements, and therefore, fracture toughness results are reported as $K_Q = K_{IC}$. Value found for neat 3D printed PLA, 2.25 ± 0.26 MPa $m^{1/2}$, are consistent with the ones found in literature for similar kind of materials and manufacturing technique [53, 55]. As shown in Fig. 13, no significative effect was observed upon the incorporation of MCC and MAH on the fracture toughness of the 3D printed material along the interlaminar plane. A worsening effect was found for PLAgMAH_10MCC (Fig. 13b), p value = 7e−4, that could be caused by the increased hardship found in printing that particular material and its brittle behavior.

4 Conclusions

In this work, filaments based on poly (lactic acid) (PLA) and micro crystalline cellulose (MCC) were prepared by a two-step process (compounding and extrusion) and used to produce samples by fused filament fabrication. The effect of the addition of a compatibilizer agent was studied. In fact, maleic anhydride was grafted on PLA in a melt compounder with the aid of a peroxide. To improve the dispersion of the filler in the polymer matrix, two different types of masterbatch biocomposite were prepared at 10wt.% of MCC, with or without MAH, i.e., PLAgMAH/MCC and PLA/MCC. Micro composite filaments were fabricated with the aid of a single screw extruder and then deposited through a 3D printer to form the final specimen. The grafting of maleic anhydride on PLA was proved through infrared spectroscopy that evidenced the presence of peaks related to the bonding of MAH. Electron microscopy was used to investigate the filler–matrix interaction and it highlighted, that upon the addition of maleic anhydride on the PLA backbone, an important improve moving from an incoherent interphase to a coherent one that suggested a good adhesion of MCC. No particular effects on the thermal degradation of PLA were revealed by thermal gravimetric analysis upon the addition of maleic anhydride and micro cellulose. According to differential scanning calorimetry analysis, micro-cellulose acted as nucleating agent for PLA shifting towards lowers temperature the crystallization peak and was observed a synergistic effect when MCC was added to PLA grafted with MAH possibly due to the increase of the chain mobility due to the low molecular weight of MAH. Stiffness of filaments was increased by the presence of micro cellulose but at the same time an embrittlement of the material was observed, this effect was amplified by the grafting with MAH. 3D printed samples demonstrated an increase in stiffness with the increasing amount of micro-cellulose

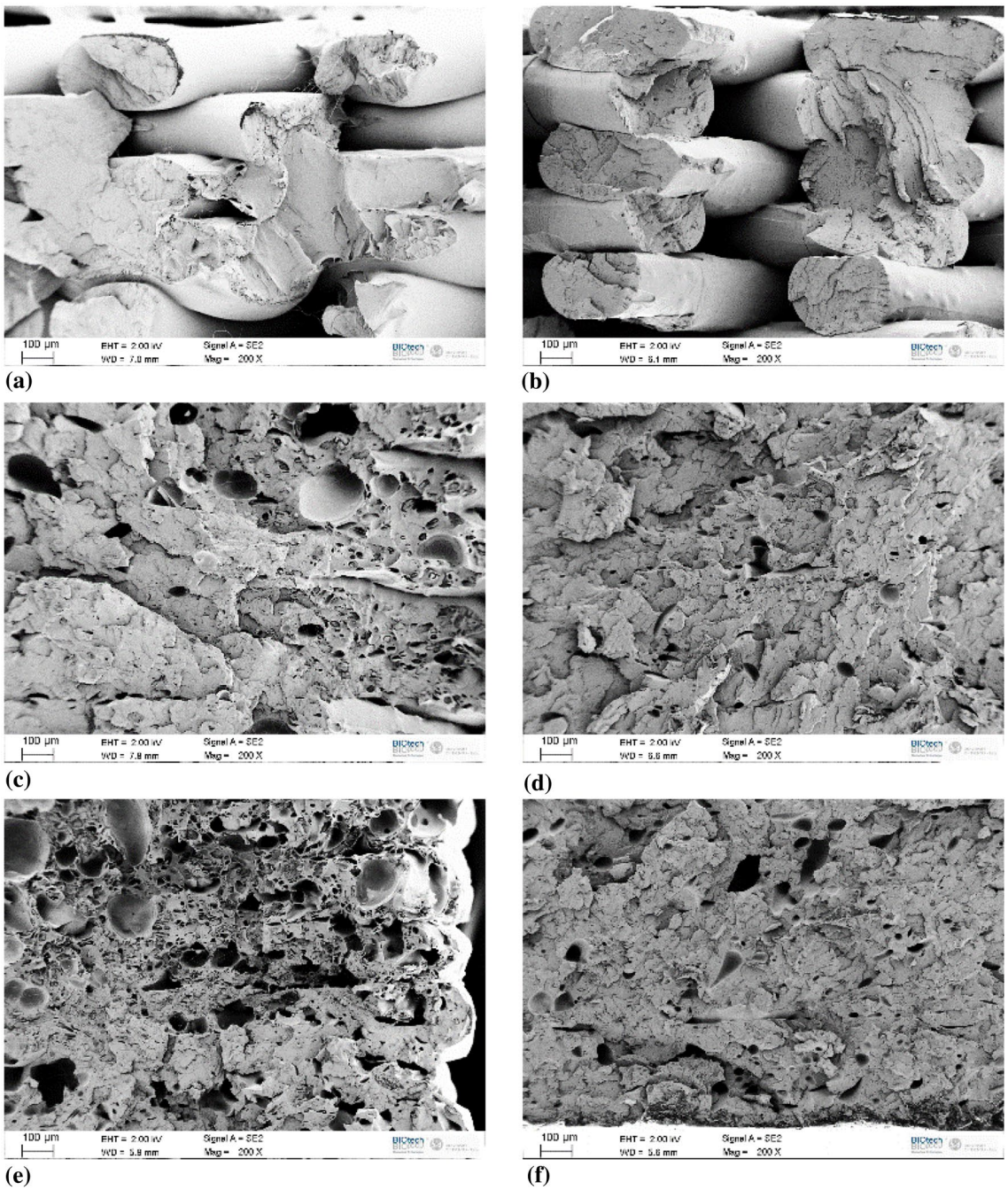

Fig. 11 SEM pictures of the fracture surface after tensile test on neat PLA (**a**), PLAgMAH_01MCC (**b**), PLA_05MCC (**c**), PLAgMAH_05MCC (**d**), PLA_10MCC (**e**) and PLAgMAH_10MCC (**f**)

and a different fracture behavior compared to bulk material due to the unique manufacturing process. The decrease in viscosity upon the addition of MCC and MAH could have enhanced the intra- and inter-layers adhesion, improving the mechanical properties at fracture of 3D printing samples. MAH was able to improve the interphase between PLA and

Table 3 Density of the filaments (bulk density) and apparent density of 3D printed specimens

	Bulk density (g/cm^3)	Apparent density (g/cm^3)
PLA	1.251 ± 0.057	0.689 ± 0.031
PLA_01MCC	1.241 ± 0.028	0.784 ± 0.018
PLAgMAH_01MCC	1.247 ± 0.005	0.717 ± 0.003
PLA_03MCC	1.235 ± 0.014	0.639 ± 0.007
PLAgMAH_03MCC	1.240 ± 0.021	0.802 ± 0.014
PLA_05MCC	1.221 ± 0.030	0.795 ± 0.020
PLAgMAH_05MCC	1.220 ± 0.045	0.822 ± 0.030
PLA_10MCC	1.234 ± 0.008	0.655 ± 0.004
PLAgMAH_10MCC	1.265 ± 0.008	0.799 ± 0.005

MCC, as evidenced by SEM analysis, and, therefore, grafted maleic anhydride onto polylactide has been confirmed, to be a good compatibilizer to improve the adhesion of cellulose to the PLA matrix. Finally, a R-factor, defined by the ratio of apparent and bulk density, could be a useful indicator of the suitability of the investigated material for the FFF technology. It was found to be positively affected by the presence of MAH that could have improved the easiness of the printing process. Mechanical properties that depend on the cross section of specimen was also found to be related to R according to ANOVA. Interlayer fracture toughness was found to not be related by the presence of MCC in presence or not of MAH. Following these findings, composition at 3wt% and 5wt% of MCC in presence of grafted maleic anhydride could

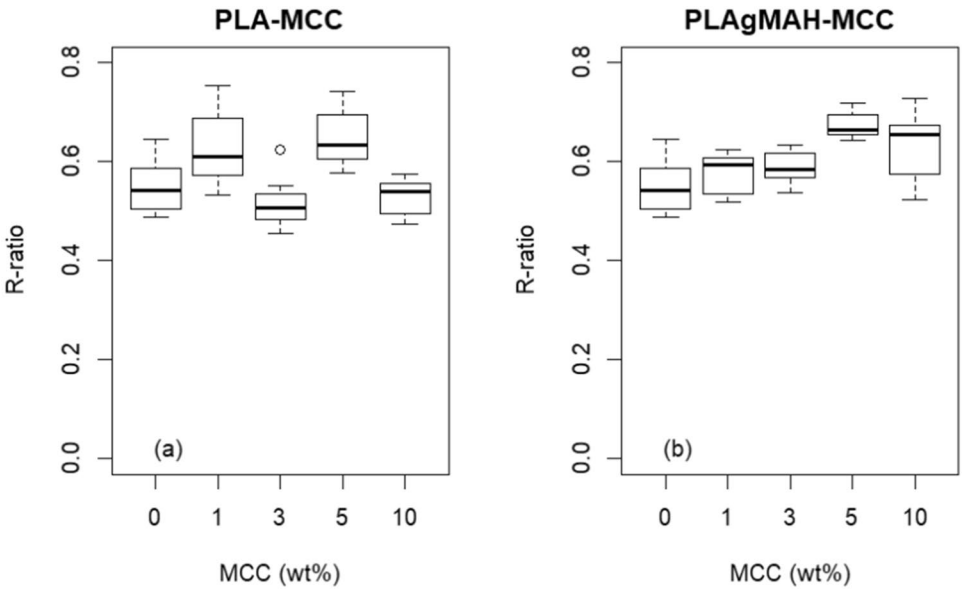

Fig. 12 R-ratio as a function of wt% of MCC for PLA (**a**) and PLA grafted MAH (**b**)

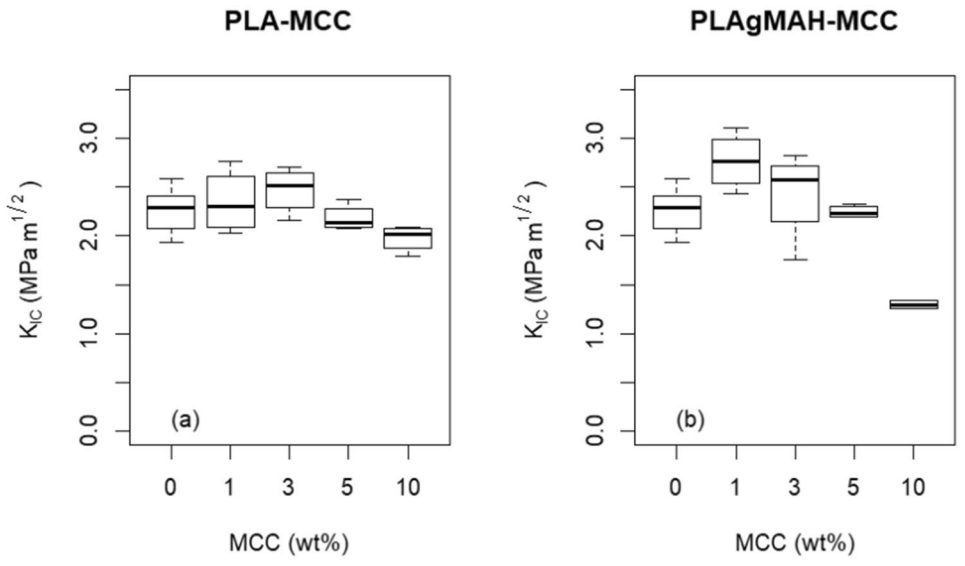

Fig. 13 Critical stress intensity factor for 3D printed PLA (**a**) and PLAgMAH (**b**) with increasing amount of MCC

be suggested for the production of 3D printed specimens, as a good compromise of processing conditions, morphological structure and mechanical properties.

Author contributions All authors contributed to the study conception and design. Material preparation, data collection and analysis were performed by DR. The first draft of the manuscript was written by DR and all authors commented on previous versions of the manuscript. All authors read and approved the final manuscript.

Funding The authors did not receive support from any organization for the submitted work.

Availability of data and materials Experimental data are available from https://archive.materialscloud.org/deposit/records/1009

Code availability Not applicable.

Declarations

Conflict of interest The authors have no conflicts of interest to declare that are relevant to the content of this article.

Additional declarations for articles in life science journals that report the results of studies involving humans and/or animals Not applicable.

Ethics approval The authors certify that they have NO affiliations with or involvement in any organization or entity with any financial interest (such as honoraria; educational grants; participation in speakers' bureaus; membership, employment, consultancies, stock ownership, or other equity interest; and expert testimony or patent-licensing arrangements), or non-financial interest (such as personal or professional relationships, affiliations, knowledge or beliefs) in the subject matter or materials discussed in this manuscript.

Consent to participate Not applicable.

Consent for publication The authors consent the publication of this research.

References

1. Liu J, Sun L, Xu W, Wang Q, Yu S, Sun J (2019) Current advances and future perspectives of 3D printing natural-derived biopolymers. Carbohydr Polym 207:297–316. https://doi.org/10.1016/j.carbpol.2018.11.077
2. Ngo TD, Kashani A, Imbalzano G, Nguyen KTQ, Hui D (2018) Additive manufacturing (3D printing): a review of materials, methods, applications and challenges. Compos B Eng 143:172–196. https://doi.org/10.1016/j.compositesb.2018.02.012
3. Ghilan A, Chiriac AP, Nita LE, Rusu AG, Neamtu I, Chiriac VM (2020) Trends in 3D printing processes for biomedical field: opportunities and challenges. J Polym Environ 28(5):1345–1367. https://doi.org/10.1007/s10924-020-01722-x
4. Singh R, Singh J, Singh S (2016) Investigation for dimensional accuracy of AMC prepared by FDM assisted investment casting using nylon-6 waste based reinforced filament. Measurement 78:253–259. https://doi.org/10.1016/j.measurement.2015.10.016
5. Chong S, Pan G-T, Khalid M, Yang TCK, Hung S-T, Huang C-M (2017) Physical characterization and pre-assessment of recycled high-density polyethylene as 3D printing material. J Polym Environ 25(2):136–145. https://doi.org/10.1007/s10924-016-0793-4
6. Dul S, Fambri L, Pegoretti A (2016) Fused deposition modelling with ABS–graphene nanocomposites. Compos A Appl Sci Manuf 85:181–191. https://doi.org/10.1016/j.compositesa.2016.03.013
7. Byberg KI, Gebisa AW, Lemu HG (2018) Mechanical properties of ULTEM 9085 material processed by fused deposition modeling. Polym Test 72:335–347. https://doi.org/10.1016/j.polymertesting.2018.10.040
8. Rigotti D, Dorigato A, Pegoretti A (2018) 3D printable thermoplastic polyurethane blends with thermal energy storage/release capabilities. Mater Today Commun 15:228–235. https://doi.org/10.1016/j.mtcomm.2018.03.009
9. Cataldi A, Rigotti D, Nguyen VDH, Pegoretti A (2018) Polyvinyl alcohol reinforced with crystalline nanocellulose for 3D printing application. Mater Today Commun 15:236–244. https://doi.org/10.1016/j.mtcomm.2018.02.007
10. Chen Z, Li Z, Li J, Liu C, Lao C, Fu Y, Liu C, Li Y, Wang P, He Y (2019) 3D printing of ceramics: a review. J Eur Ceram Soc 39(4):661–687. https://doi.org/10.1016/j.jeurceramsoc.2018.11.013
11. Bourell D, Kruth JP, Leu M, Levy G, Rosen D, Beese AM, Clare A (2017) Materials for additive manufacturing. CIRP Ann 66(2):659–681. https://doi.org/10.1016/j.cirp.2017.05.009
12. Xu J, Ding L, Cai L, Zhang L, Luo H, Qin W (2019) Volume-forming 3D concrete printing using a variable-size square nozzle. Autom Constr 104:95–106. https://doi.org/10.1016/j.autcon.2019.03.008
13. Liu Z, Wang Y, Wu B, Cui C, Guo Y, Yan C (2019) A critical review of fused deposition modeling 3D printing technology in manufacturing polylactic acid parts. Int J Adv Manuf Technol 102(9–12):2877–2889. https://doi.org/10.1007/s00170-019-03332-x
14. Pegoretti A, Fambri L, Migliaresi C (1997) In vitro degradation of poly(L-lactic acid) fibers produced by melt spinning. J Appl Polym Sci 64(2):213–223. https://doi.org/10.1002/(Sici)1097-4628(19970411)64:2%3c213::Aid-App2%3e3.3.Co;2-H
15. Sun J, Shen J, Chen S, Cooper M, Fu H, Wu D, Yang Z (2018) Nanofiller reinforced biodegradable PLA/PHA composites: current status and future trends. Polymers 10(5):505
16. Swaroop C, Shukla M (2018) Nano-magnesium oxide reinforced polylactic acid biofilms for food packaging applications. Int J Biol Macromol 113:729–736. https://doi.org/10.1016/j.ijbiomac.2018.02.156
17. Murariu M, Dubois P (2016) PLA composites: From production to properties. Adv Drug Deliv Rev 107:17–46. https://doi.org/10.1016/j.addr.2016.04.003
18. Oksman K, Skrifvars M, Selin JF (2003) Natural fibres as reinforcement in polylactic acid (PLA) composites. Compos Sci Technol 63(9):1317–1324. https://doi.org/10.1016/s0266-3538(03)00103-9
19. Mathew AP, Oksman K, Sain M (2005) Mechanical properties of biodegradable composites from poly lactic acid (PLA) and microcrystalline cellulose (MCC). J Appl Polym Sci 97(5):2014–2025. https://doi.org/10.1002/app.21779
20. Abdul Khalil HPS, Bhat AH, Ireana Yusra AF (2012) Green composites from sustainable cellulose nanofibrils: a review. Carbohydr Polym 87(2):963–979. https://doi.org/10.1016/j.carbpol.2011.08.078
21. Rzayev Z (2011) Graft copolymers of maleic anhydride and its isostructural analogues: high performance engineering materials. High Performance Engineering Materials. 1105.1260

22. Hwang SW, Lee SB, Lee CK, Lee JY, Shim JK, Selke SEM, Soto-Valdez H, Matuana L, Rubino M, Auras R (2012) Grafting of maleic anhydride on poly(L-lactic acid). Effects on physical and mechanical properties. Polym Test 31(2):333–344. https://doi.org/10.1016/j.polymertesting.2011.12.005
23. Issaadi K, Habi A, Grohens Y, Pillin I (2015) Effect of the montmorillonite intercalant and anhydride maleic grafting on polylactic acid structure and properties. Appl Clay Sci 107:62–69. https://doi.org/10.1016/j.clay.2015.01.004
24. Detyothin S, Selke SEM, Narayan R, Rubino M, Auras R (2013) Reactive functionalization of poly(lactic acid), PLA: effects of the reactive modifier, initiator and processing conditions on the final grafted maleic anhydride content and molecular weight of PLA. Polym Degrad Stab 98(12):2697–2708. https://doi.org/10.1016/j.polymdegradstab.2013.10.001
25. Ma P, Jiang L, Ye T, Dong W, Chen M (2014) Melt free-radical grafting of maleic anhydride onto biodegradable poly(lactic acid) by using styrene as a comonomer. Polymers 6(5):1528–1543. https://doi.org/10.3390/polym6051528
26. Kaynak C, Meyva Y (2014) Use of maleic anhydride compatibilization to improve toughness and other properties of polylactide blended with thermoplastic elastomers. Polym Adv Technol 25(12):1622–1632. https://doi.org/10.1002/pat.3415
27. Petersson L, Oksman K, Mathew AP (2006) Using maleic anhydride grafted poly(lactic acid) as a compatibilizer in poly(lactic acid)/layered-silicate nanocomposites. J Appl Polym Sci 102(2):1852–1862. https://doi.org/10.1002/app.24121
28. Tsou C-H, Hung W-S, Wu C-S, Chen J-C, Huang C-Y, Chiu S-H, Tsou C-Y, Yao W-H, Lin S-M, Chu C-K, Hu C-C, Lee K-R, Suen M-C (2014) New composition of maleic-anhydride-grafted poly(lactic acid)/rice husk with methylenediphenyl diisocyanate. Mater Sci. https://doi.org/10.5755/j01.ms.20.4.6034
29. Zhu R, Liu H, Zhang J (2012) Compatibilizing effects of maleated poly(lactic acid) (PLA) on properties of PLA/soy protein composites. Ind Eng Chem Res 51(22):7786–7792. https://doi.org/10.1021/ie300118x
30. Nyambo C, Mohanty AK, Misra M (2011) Effect of maleated compatibilizer on performance of PLA/wheat straw-based green composites. Macromol Mater Eng 296(8):710–718. https://doi.org/10.1002/mame.201000403
31. Zhang JF, Sun X (2004) Physical characterization of coupled poly(lactic acid)/starch/maleic anhydride blends plasticized by acetyl triethyl citrate. Macromol Biosci 4(11):1053–1060. https://doi.org/10.1002/mabi.200400076
32. Siró I, Plackett D (2010) Microfibrillated cellulose and new nanocomposite materials: a review. Cellulose 17(3):459–494. https://doi.org/10.1007/s10570-010-9405-y
33. Rigotti D, Checchetto R, Tarter S, Caretti D, Rizzuto M, Fambri L, Pegoretti A (2019) Polylactic acid-lauryl functionalized nanocellulose nanocomposites: microstructural, thermo-mechanical and gas transport properties. Express Polym Lett 13(10):858–876. https://doi.org/10.3144/expresspolymlett.2019.75
34. Spinella S, Lo Re G, Liu B, Dorgan J, Habibi Y, Leclère P, Raquez J-M, Dubois P, Gross RA (2015) Polylactide/cellulose nanocrystal nanocomposites: efficient routes for nanofiber modification and effects of nanofiber chemistry on PLA reinforcement. Polymer 65:9–17. https://doi.org/10.1016/j.polymer.2015.02.048
35. Wen H, Wang Y, Wang D, de Claville Christiansen J, Yu D, Jiang S, Chen C (2019) Evaluation of relationship between crystallization structure and thermal-mechanical performance of PLA with MCC addition. ChemistrySelect 4(34):10174–10180. https://doi.org/10.1002/slct.201902015
36. Valentini F, Dorigato A, Rigotti D, Pegoretti A (2019) Polyhydroxyalkanoates/fibrillated nanocellulose composites for additive manufacturing. J Polym Environ 27(6):1333–1341. https://doi.org/10.1007/s10924-019-01429-8
37. Fortunati E, Luzi F, Puglia D, Dominici F, Santulli C, Kenny JM, Torre L (2014) Investigation of thermo-mechanical, chemical and degradative properties of PLA-limonene films reinforced with cellulose nanocrystals extracted from phormium tenax leaves. Eur Polym J 56:77–91. https://doi.org/10.1016/j.eurpolymj.2014.03.030
38. Song X, He W, Han X, Qin H (2020) Fused deposition modeling of poly (lactic acid)/nutshells composite filaments: effect of alkali treatment. J Polym Environ 28(12):3139–3152. https://doi.org/10.1007/s10924-020-01839-z
39. Fischer EW, Sterzel HJ, Wegner G (1973) Investigation of the structure of solution grown crystals of lactide copolymers by means of chemical reactions. Kolloid-Zeitschrift und Zeitschrift für Polymere 251(11):980–990. https://doi.org/10.1007/bf01498927
40. Technical datasheet Available from: https://www.sigmaaldrich.com/IT/it/product/aldrich/m188
41. Zhou L, He H, Li M-C, Huang S, Mei C, Wu Q (2018) Enhancing mechanical properties of poly(lactic acid) through its in-situ crosslinking with maleic anhydride-modified cellulose nanocrystals from cottonseed hulls. Ind Crops Prod 112:449–459. https://doi.org/10.1016/j.indcrop.2017.12.044
42. Yu T, Jiang N, Li Y (2014) Study on short ramie fiber/poly(lactic acid) composites compatibilized by maleic anhydride. Compos A Appl Sci Manuf 64:139–146. https://doi.org/10.1016/j.compositesa.2014.05.008
43. Cooper-White JJ, Mackay ME (1999) Rheological properties of poly(lactides). Effect of molecular weight and temperature on the viscoelasticity of poly(L-lactic acid). J Polym Sci Part B Polym Phys 37(15):1803–1814. https://doi.org/10.1002/(sici)1099-0488(19990801)37:15<1803::aid-polb5>3.0.co;2-m
44. Barczewski M, Mysiukiewicz O (2018) Rheological and processing properties of poly(lactic acid) composites filled with ground chestnut shell. Polymer Korea 42:267–274. https://doi.org/10.7317/pk.2018.42.2.267
45. Brian NT (2014) A review of melt extrusion additive manufacturing processes. I. Process design and modeling. Rapid Prototyp J 20(3):192–204. https://doi.org/10.1108/RPJ-01-2013-0012
46. Wang T, Drzal LT (2012) Cellulose-nanofiber-reinforced poly(lactic acid) composites prepared by a water-based approach. ACS Appl Mater Interfaces 4(10):5079–5085. https://doi.org/10.1021/am301438g
47. Khoo RZ, Ismail H, Chow WS (2016) Thermal and morphological properties of poly (lactic acid)/nanocellulose nanocomposites. Procedia Chem 19:788–794. https://doi.org/10.1016/j.proche.2016.03.086
48. Du Y, Wu T, Yan N, Kortschot MT, Farnood R (2014) Fabrication and characterization of fully biodegradable natural fiber-reinforced poly(lactic acid) composites. Compos B Eng 56:717–723. https://doi.org/10.1016/j.compositesb.2013.09.012
49. Viikna A, Krumme A, Tarasova E, Šumigin D (2012) Influence of cellulose content on thermal properties of poly(lactic) acid/cellulose and low-density polyethylene/cellulose composites. Proc Est Acad Sci 61(3):237. https://doi.org/10.3176/proc.2012.3.14
50. Frone AN, Berlioz S, Chailan JF, Panaitescu DM (2013) Morphology and thermal properties of PLA-cellulose nanofibers composites. Carbohydr Polym 91(1):377–384. https://doi.org/10.1016/j.carbpol.2012.08.054
51. Halász K, Csóka L (2013) Plasticized biodegradable poly(lactic acid) based composites containing cellulose in micro- and nano-size. J Eng 2013:1–9. https://doi.org/10.1155/2013/329379
52. Papon EA, Haque A (2019) Fracture toughness of additively manufactured carbon fiber reinforced composites. Addit Manuf 26:41–52. https://doi.org/10.1016/j.addma.2018.12.010

53. Cicero S, Martínez-Mata V, Castanon-Jano L, Alonso-Estebanez A, Arroyo B (2021) Analysis of notch effect in the fracture behaviour of additively manufactured PLA and graphene reinforced PLA. Theor Appl Fract Mech 114:103032. https://doi.org/10.1016/j.tafmec.2021.103032
54. Hart KR, Dunn RM, Wetzel ED (2020) Increased fracture toughness of additively manufactured semi-crystalline thermoplastics via thermal annealing. Polymer 211:123091. https://doi.org/10.1016/j.polymer.2020.123091
55. Chen J, Zhang T-Y, Jin F-L, Park S-J (2018) Fracture toughness improvement of poly(lactic acid) reinforced with poly(ε-caprolactone) and surface-modified silicon carbide. Adv Mater Sci Eng 2018:6537621. https://doi.org/10.1155/2018/6537621

Authors and Affiliations

Daniele Rigotti[1] · Luca Fambri[1] · Alessandro Pegoretti[1]

✉ Daniele Rigotti
daniele.rigotti-1@unitn.it

[1] Department of Industrial Engineering and INSTM Research Unit, University of Trento, Via Sommarive 9, 38123 Trento, Italy